Journal of Vacuum Science and Technology A

RESEARCH ARTICLE | AUGUST 21 2024

Tuning microstructural and oxidative characteristics of direct current- and high-power pulsed magnetron sputtered $MoSi_2$-based thin films

Special Collection: Celebrating the Achievements and Life of Joe Greene

Sophie Richter ; Ahmed Bahr ; Philip Kutrowatz; Tomasz Wojcik ; Szilárd Kolozsvári ; Peter Polcik ; Carmen Jerg ; Jürgen Ramm ; Helmut Riedl

J. Vac. Sci. Technol. A 42, 053407 (2024)
https://doi.org/10.1116/6.0003833

JVST A
Journal of Vacuum Science & Technology A

ARTICLE

pubs.aip.org/avs/jva

Tuning microstructural and oxidative characteristics of direct current- and high-power pulsed magnetron sputtered $MoSi_2$-based thin films

Cite as: J. Vac. Sci. Technol. A **42**, 053407 (2024); doi: 10.1116/6.0003833
Submitted: 16 June 2024 · Accepted: 31 July 2024 ·
Published Online: 21 August 2024

View Online Export Citation CrossMark

Sophie Richter,[1,a)] Ahmed Bahr,[1] Philip Kutrowatz,[1] Tomasz Wojcik,[1] Szilárd Kolozsvári,[2] Peter Polcik,[2] Carmen Jerg,[3] Jürgen Ramm,[3] and Helmut Riedl[1,4]

AFFILIATIONS

[1]Christian Doppler Laboratory for Surface Engineering of High-Performance Components, TU Wien, A-1060 Wien, Austria
[2]Plansee Composite Materials GmbH, D-86983 Lechbruck am See, Germany
[3]Oerlikon Balzers, Oerlikon Surface Solutions AG, FL-9496 Balzers, Liechtenstein
[4]Institute of Materials Science and Technology, TU Wien, A-1060 Wien, Austria

Note: This paper is part of the Special Topic Collection Celebrating the Achievements and Life of Joe Greene.
[a)]**Author to whom correspondence should be addressed:** sophie.richter@tuwien.ac.at

ABSTRACT

A comparative study on nonreactively direct current magnetron sputtered (DCMS) and high-power pulsed magnetron sputtered (HPPMS) $MoSi_2$-based coatings has been implemented with the objective of advancing the knowledge on the growth conditions and oxidation resistance of $MoSi_2$ thin films. The energy supplied during the growth process (i.e., deposition temperature and ionization degree) exerts a significant influence on the phase formation and morphology. At 200 °C, highly dense but x-ray amorphous films are prevalent, whereas an increase up to 400 °C leads to dense and fine-columnar structured hexagonal $MoSi_2$ films. Increased growth temperatures (≥500 °C for DCMS) and strongly ionized plasma states result in the formation of dual-phase structures (h-$MoSi_2$ and t-Mo_5Si_3), accompanied by slightly underdense but strongly columnar grains. The $MoSi_{1.92}$ HPPMS film (1000 Hz, 10% duty cycle) grown at 500 °C exhibits the maximum hardness of 22.8 GPa and an elastic modulus of approximately 400 GPa. In long-term oxidation tests conducted at 600, 850, and 1200 °C (up to 100 h), all $MoSi_2$-based films exhibited a temperature-dependent scale formation. Up to 850 °C, the formation of a continuous, dense protective scale is disrupted by the competing growth of MoO_x and SiO_x. At temperatures exceeding 1200 °C, all $MoSi_2$-based coatings analyzed demonstrate exceptional oxidation resistance, resulting in the formation of a continuous, dense SiO_2 scale. At 1500 °C for 30 min, the initially slightly underdense and dual-phased $MoSi_{1.92}$ coating achieved a scale thickness of only 670 nm, thereby demonstrating the exceptional oxidation resistance capabilities of HPPMS-grown $MoSi_2$-based coatings.

I. INTRODUCTION

The potential of intermetallic Mo-Si compounds as ultrahigh temperature materials has attracted the attention of researchers due to their exceptional thermal properties beyond 1600 °C.[1] Given their versatile properties, including extremely high phase stability, tribological characteristics,[2,3] and optoelectronic properties,[4,5] Mo-Si-based materials are suitable for a wide range of applications. The binary Mo-Si system comprises three distinct intermetallic compounds: $MoSi_2$, Mo_5Si_3, and Mo_3Si, respectively. While the Mo-rich phases, such as Mo_5Si_3 and Mo_3Si, exhibit superior

mechanical properties, the Si-rich phase, $MoSi_2$, displays enhanced oxidation resistance.[1] The oxidation behavior of $MoSi_2$ has been extensively studied for bulk materials, with the formation of a highly protective silica scale (SiO_2) being responsible for the enhanced oxidation resistance.[6–9] It is evident that $MoSi_2$ materials display unfavorable oxidation resistance at low temperatures (below 600 °C), which can be attributed to the so-called pesting phenomenon, well-known for Mo-based alloys.[10–12] The pesting phenomenon typically manifests when mixed oxides (e.g., metallic and silica-based) grow simultaneously, resulting in internal stresses due to the significant volume expansion of the respective oxides.[8] A substantial body of research has demonstrated that microstructure and structural defects exert a profound influence on the pesting behavior of $MoSi_2$ bulk and coating materials. Typically, accelerated oxidation occurs as a result of the formation of cracks and pores, which leads to the formation of a poorly protective and porous oxide layer comprising mixed amorphous Si- and Mo-containing oxidation products.[13,14] Nevertheless, the remarkable high-temperature oxidation resistance of $MoSi_2$—which forms a dense and protective scale that inhibits oxygen inward diffusion up to 1400 °C—indicates that it is a promising candidate for applications at elevated temperatures.[15]

The value of this feature has been demonstrated in numerous studies of $MoSi_2$ coating materials produced through a variety of deposition techniques, including chemical vapor deposition,[16] as well as vacuum and atmospheric plasma spraying.[17–20] Nevertheless, these deposition techniques are not without limitations. In plasma spraying, the unintended addition of oxygen during film growth, which is provided by atmospheric conditions, weakens the protective effect of the coatings with regard to oxygen. Moreover, the formation of a uniform $MoSi_2$ phase throughout the entire film thickness has not been demonstrated to be a straightforward process in hot dipping siliconizing.[21] This inconsistency results in a limited oxidation resistance, as reported by Liu *et al.*[22] Magnetron sputtering, a physical vapor deposition (PVD) technique, represents an alternative approach for the synthesis of $MoSi_2$ thin films. While the existing literature addresses the mechanical properties and phase formation of direct current magnetron sputtered (DCMS) $MoSi_2$ thin films,[23–25] there are no reports on the growth of $MoSi_2$ films using other PVD methods, such as high-power pulsed magnetron sputtering (HPPMS). In the comparative study conducted by Bahr *et al.*, DCMS-grown $TaSi_2$, $NbSi_2$, and $MoSi_2$ were primarily investigated with regard to long-term oxidation kinetics at 1200 °C.[15]

In the context of oxidation resistance, HPPMS-grown $MoSi_2$ thin films are of interest as highly ionized plasmas have the potential to positively influence the microstructure. A densified and more perfect morphology may prove to be a crucial factor during scale formation (e.g., pesting behavior) and retarded oxygen inward diffusion. The objective of this study is to gain a deeper understanding of the growth and oxidation characteristics of nonreactively sputtered $MoSi_2$ thin films using different sputtering techniques (i.e., HPPMS versus DCMS). Furthermore, the objective is to examine the coating performance of even higher oxidation temperatures, up to 1500 °C, with the aim of providing a comprehensive characterization of the observed phenomena.

II. EXPERIMENTAL

A. Deposition process

All $MoSi_2$-based thin films were synthesized in a laboratory-scale magnetron sputtering system. A 3″ $MoSi_2$ compound target with a purity of 99.34%, provided by Plansee Composite Materials GmbH,[26] was operated in DC- and HPPMS modes with 99.999% pure argon as the working gas. Prior to all deposition processes, a base pressure of less than 4×10^{-4} Pa was attained. For DCMS depositions, the substrate temperature was varied from 200 to 600 °C, while the bias potential was maintained at −50 V. The target power density for DCMS was kept at 5.6 W/cm^2, and the deposition pressure was set at 0.4 Pa by introducing 21 sccm of argon. Moreover, two HPPMS series were synthesized, with the frequencies varying from 500 to 1000 Hz, and the pulse duty cycles (t_{on}/T) adjusted to 2.5%, 5%, and 10%, respectively. All HPPMS films were deposited at a substrate temperature of 500 °C and a DC bias potential of −50 V. The resulting peak power density for the HPPMS films exhibited a range of 150–600 W/cm^2, based on an average power of 7.8 W/cm^2 set at the generator. The deposition pressure was maintained at a constant value of 0.4 Pa by introducing a flow rate of 21 sccm of argon. Single-crystalline silicon (100 orientation, $20 \times 7 \times 0.38$ mm), single-crystalline Al_2O_3 (sapphire, 1-102 orientation, $10 \times 10 \times 0.53$ mm), and polycrystalline Al_2O_3 ($20 \times 7 \times 0.38$ mm) substrates were positioned parallel to the target at a distance of 70 mm and rotated at 0.23 Hz. Prior to the deposition process, an ultrasonic bath was utilized to clean the substrates in acetone and ethanol for a duration of 5 min each. Subsequently, an argon ion etching step was conducted, lasting for 15 min and employing a substrate bias potential of −800 V, along with an argon flow rate of 180 sccm. The resulting etching pressure was approximately 4.9 Pa. Prior to deposition, the target surface was subjected to presputtering at a power density of approximately 2.2 W/cm^2 for the final 2 min, with the shutters closed. The deposition time for the samples in the DCMS series was 30 min, with the exception of the thin film deposited at 500 °C, which required 60 min. The deposition time for the HPPMS coatings was 60 min, except in the case of coatings deposited at 500 Hz with a 10% duty cycle, where the deposition time was 45 min. Overall, the deposition times were adjusted to achieve film thicknesses between 3 and 4 μm.

B. Coating characterization

A microstructural analysis of the $MoSi_2$ films was conducted using a scanning electron microscope (SEM) instrument of varying specifications. The analysis was performed on cross sections of the films in their both as-deposited and annealed states. The SEM instruments utilized were the FEI Quanta 200 FEGSEM, operating at 10 kV, and the Zeiss Sigma 500 VP SEM, operating at 3 kV. Additional cross sections of the oxidized samples were prepared using a dual-beam focused ion beam/scanning electron microscope (FIB-SEM) system (Thermo Scientific Scios 2). The cross sections were prepared using Ga^+ ions at an acceleration voltage of 30 kV and an ion beam current of 7–15 nA for rough milling. The final fine milling was conducted with a beam current of 1 nA. The chemical composition was analyzed by energy-dispersive x-ray

spectroscopy (EDX) using a FEI Philips XL30 scanning electron microscope (SEM) operated at an accelerating voltage of 20 kV. For the transmission electron microscopy (TEM) analysis, a FEI TECNAI F20 microscope equipped with a field emission gun was utilized to generate bright-field (BF) images. The TEM lamellas were prepared with the same dual-beam FIB-SEM system that was used for the preparation of the oxidized samples. To analyze the phase evolution of the deposited $MoSi_2$ films, a Panalytical X'Pert Pro MPD X-ray diffractometer was employed in a Bragg Brentano configuration with a Cu-Kα radiation source (wavelength $\lambda = 1.5418$ Å). All measurements on coated single-crystalline Al_2O_3 were conducted with an offset of 3° to reduce the influence of substrate peaks.

The mechanical properties, including hardness and elastic modulus, were determined by nanoindentation on sapphire substrates using an Ultra Micro Indentation System (UMIS) with a Berkovich diamond tip. In order to calculate the respective modulus, the Poisson's ratio of $MoSi_2$ was assumed to be $\nu = 0.25$. A line measurement of 30 indentations at various loads between 3 and 45 mN was conducted to ensure that the penetration depths did not exceed 10% of the film thickness, thereby minimizing the influence of the substrate. The load-displacement curves were evaluated in accordance with the methodology proposed by Oliver and Pharr.[27,28]

Long-term oxidation tests were conducted on single-crystalline Al_2O_3 substrates in ambient air at temperatures of 600, 850, and 1200 °C for 100 h in a conventional furnace. To gain further insight into the high-temperature oxidation behavior, selected coatings on polycrystalline Al_2O_3 substrates were subjected to a synthetic air atmosphere in a Netzsch STA 449 F1 setup with a rhodium furnace. The isothermal oxidation tests were conducted at temperatures of 1300, 1400, and 1500 °C. The annealing time was 60 min, except in the case of the test at 1500 °C, where the annealing time was reduced to 30 min to prevent the system and equipment from overheating. During the oxidation test, a constant supply of oxygen (50 ml/min) and helium (20 ml/min) was maintained, the latter with the objective of protecting the oxide scale formation.

III. RESULTS AND DISCUSSION

A. Phase evolution and morphology

To study the microstructure and growth morphology of the as-deposited $MoSi_2$-based thin films, SEM cross sections have been prepared for all DCMS and HPPMS coatings. Figure 1 depicts the cross-sectional morphology of the DCMS $MoSi_2$ films deposited at varying substrate temperatures (with a constant DC bias potential of −50 V for all conditions). The dashed line represents the interface between the Si substrate and the respective coatings [Figs. 1(a)–1(e)]. The chemical composition of selected coatings was determined by EDX and is presented in Fig. 1. Additional TEM lamellae were prepared for the coating deposited at 400 and 500 °C, respectively.

The cross section in Fig. 1(a) displays a featureless, dense $MoSi_2$ thin film, which exhibits a slight Si super-stoichiometry. As the substrate temperature exceeds 300 °C, the morphological appearance changes to a more columnar state, indicative of a mixed island growth mode of crystalline features, see Figs. 1(b)–1(e). In all observed columnar morphologies, the grains are arranged in a fibrous shape, perpendicular to the substrate according to the growth direction. The coatings deposited at 300 and 400 °C appear denser in comparison to those grown at higher temperatures, as the columns are closely arranged, leaving no pores. In contrast, the coatings depicted in Figs. 1(d) and 1(e) exhibit straight and more continuous columns but with small open porosities in-between. In more detail, this can be also seen by the TEM bright-field images in Fig. 1(f) (400 °C) and Fig. 1(g) (500 °C). In particular, the coating depicted in Fig. 1(g) exhibits larger and continuous columns with underdense grain boundary regions. These morphological changes are related to enhanced diffusion processes with increasing temperatures, whereas in the medium temperature range, a competitive growth between different oriented nuclei promotes the formation of densely overgrown grains. At higher temperatures, recrystallization and restructuring lead to the elimination of overgrown and closest arranged features. In accordance with the temperature-related alterations in the growth mode, the coatings deposited at 300 and 400 °C exhibit a more fine-grained morphology in the vicinity of the substrate, thereby corroborating the aforementioned competitive growth. From a compositional standpoint, a slight decline in the Si/Mo ratio can be discerned with rising temperature.

The influence of ionized species within the plasma on microstructural evolution is illustrated in Fig. 2, presenting fracture cross sections of the as-deposited HPPMS $MoSi_2$ thin films. Once more, the bias voltage and substrate temperature were maintained at 500 °C and −50 V, respectively, for all HPPMS films. The coatings depicted in Figs. 2(a)–2(c) were synthesized at a pulse frequency of 500 Hz, with duty cycles of 2.5%, 5%, and 10%, respectively (as indicated in the lower right corner of each cross section). The morphologies of these coatings are comparable to those of the DCMS coatings grown at 500 and 600 °C, as evidenced by the presence of straight columns with grain boundaries that are not fully dense. The combination of the enhanced plasma conditions accompanied by the relatively high deposition temperature predominates the growth mode. Nevertheless, increased duty cycles, such as 10%, maintain decreased peak power densities, which result in slightly denser morphologies by retarding morphological reorganization effects. Furthermore, all coatings grown at 500 Hz display slight indications of a finer morphology in the substrate interface region. In comparison, the films deposited at 1000 Hz exhibit notable differences in their appearance, as illustrated in Figs. 2(d)–2(f). The growth morphology is more densely arranged, with columns of a smaller size. The small, interrupted features suggest the presence of a more competitive growth mode involving the overgrowth of multiple nuclei, which is analogous to the DCMS coatings deposited at 300 and 400 °C. However, the mean column size appears to be even smaller.

The diverse growth conditions, encompassing the deposition temperatures for DCMS and the ionization degree through varying parameters for the HPPMS states, exert a considerable influence on the phase formation of $MoSi_2$-based thin films. The phase evolution of all as-deposited thin films was investigated via x-ray diffraction in Bragg–Brentano geometry (offset of 3°) on single-crystalline Al_2O_3 substrates, as illustrated in Fig. 3.

While an x-ray amorphous state was only observed for the films grown at 200 °C, higher deposition temperatures resulted in

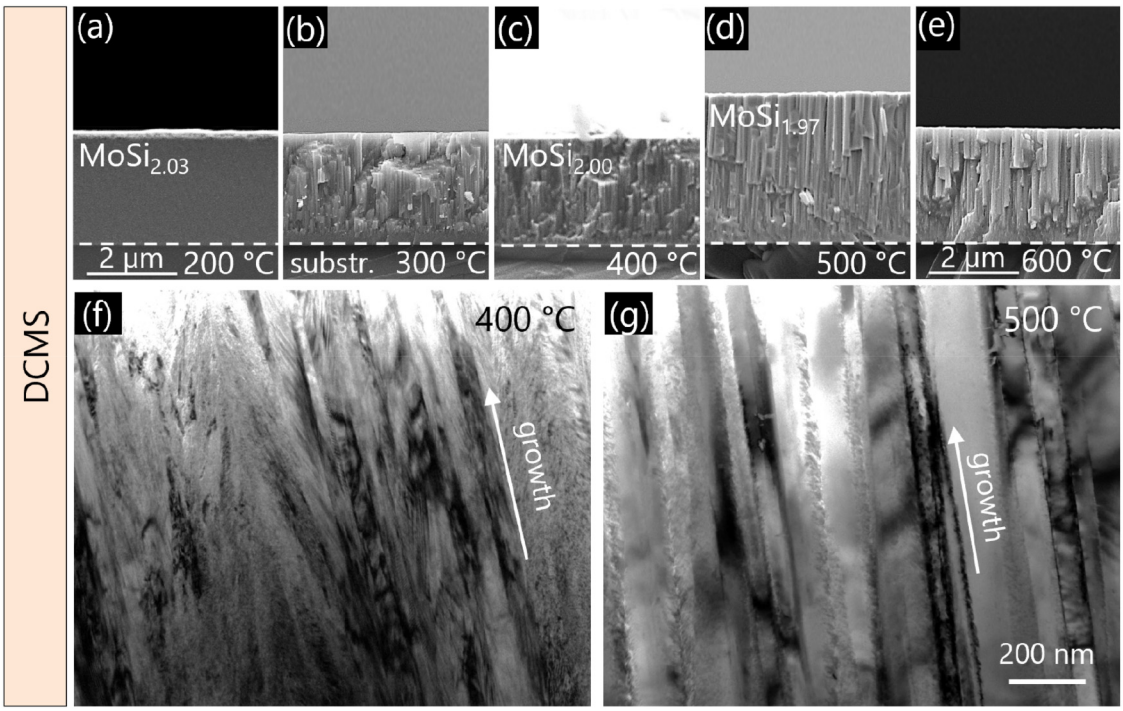

FIG. 1. SEM cross sections of the as-deposited DCMS $MoSi_2$-based thin films at different substrate temperatures are presented, with the chemical compositions (analyzed by EDX) indicated for selected states. The temperatures are (a) 200, (b) 300, (c) 400, (d) 500, and (e) 600 °C, respectively. Additional TEM cross sections are presented in (f) and (g), which depict the coatings deposited at 400 and 500 °C, respectively.

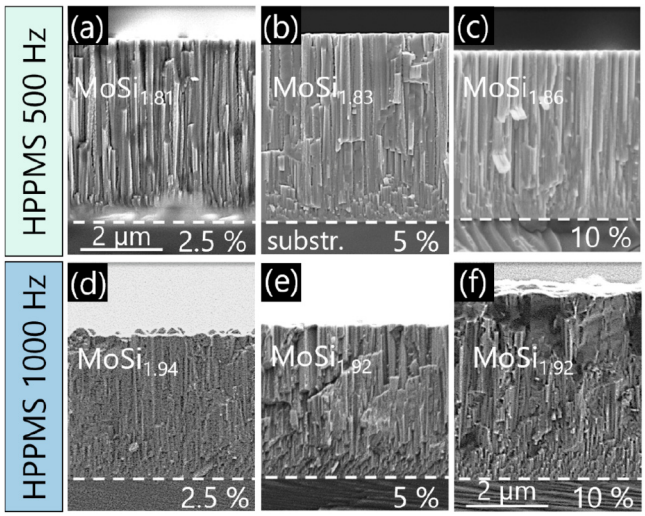

FIG. 2. SEM cross sections of the as-deposited HPPMS $MoSi_2$ thin films. The specific HPPMS parameters utilized are indicated on the left-hand side of the figure as well as within the cross sections. The first line represents the 500 Hz sample synthesized with a (a) 2.5%, (b) 5%, and (c) 10% duty cycle, respectively. The second line displays the 1000 Hz sample, again with a (d) 2.5%, (e) 5%, and (f) 10% duty cycle, respectively. The interface between the substrate (Si) and the coating is delineated by the dashed line.

the formation of single- or dual-phase structures. The predominant phases are also indicated on the right-hand side of all diffractograms. The evident structural evolution from x-ray amorphous to a single-crystalline hexagonal (h) $MoSi_2$ phase at 300 °C is in accordance with the morphology observed in Fig. 1.

At temperatures between 300 and 400 °C, the $MoSi_2$-based films can be assigned to the metastable h-$MoSi_2$ phase. Nevertheless, there are already peak overlaps with Mo_5Si_3, as evidenced by the peak observed at 26.1°. However, all other orientations exhibit perfect alignment with the hexagonal structure, and the observed stoichiometry strongly suggests the formation of the h-$MoSi_2$ phase. Even so, there is a slight indication of the formation of the tetragonal (t) Mo_5Si_3 phase, albeit in small quantities, at 29°. Moreover, the metastable h-$MoSi_2$ phase exhibits different orientations as a result of a predominant competitive growth mode.

An additional increase in deposition temperature results in the formation of a dual-phase structure comprising h-$MoSi_2$ and t-Mo_5Si_3, which aligns with the chemical changes observed in Fig. 1. This trend is also observed in the peak intensities of the Mo_5Si_3 phase, which increases with temperature. The pronounced preferred orientation of the 600 °C film at 41.5° is particularly noteworthy, aligning with the morphological changes observed (Fig. 1). However, due to peak overlap, it is challenging to definitely assign a specific phase. This is because the (202) orientation of the t-Mo_5Si_3 phase partially overlaps with the (111) h-$MoSi_2$ phase. Nevertheless, a more detailed examination of the peak shoulder

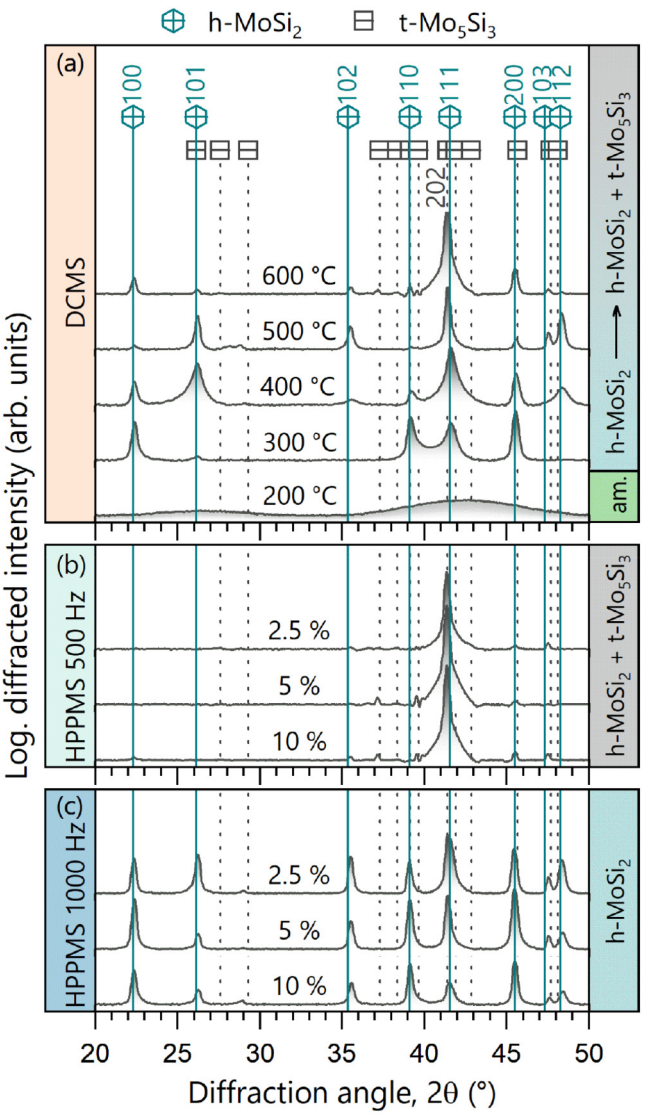

FIG. 3. X-ray diffractograms of the as-deposited $MoSi_2$ coatings are presented in (a) as a function of the substrate temperature during DCMS deposition. The various HPPMS films are illustrated in (b) for 500 Hz and (c) for 1000 Hz, with different duty cycles varying from 2.5% to 10%, respectively. The reference patterns for the hexagonal beta $MoSi_2$ (C40, $CrSi_2$ prototype) phases are represented by hexagons and continuous lines, as referenced in Ref. 29, whereas the tetragonal Mo_5Si_3 (D8 m, W_5Si_3 prototype) phase is labeled by squares with dashed lines, as referenced in Ref. 30.

indicates the presence of a dual-phase structure. Furthermore, the tetragonal Mo_5Si_3 phase is thermodynamically stable, and there is a tendency for Si to form substoichiometric compositions at higher temperatures.[15]

Figures 3(b) and 3(c) illustrate the phase evolution of the HPPMS coatings. In accordance with their morphological appearance, the 500 Hz coatings also exhibit comparable crystal structures and diffractograms to those of the DCMS grown at 600 °C. All coating states are predominantly dual-phase structured, comprising primarily h-$MoSi_2$ and t-Mo_5Si_3. The predominant growth orientation (as indicated by the peak at 41.5°) is consistent with the observed pronounced columnar morphology. In contrast, the 1000 Hz HPPMS coatings obtain h-$MoSi_2$ predominated structures with small indications of the t-Mo_5Si_3 phase for the 2.5% and 10% duty cycle states, respectively. All three coatings grown at 1000 Hz exhibit a random oriented structure [see Fig. 3(c)].

B. Mechanical properties

The morphological and structural differences of the as-deposited $MoSi_2$ films, resulting from the distinct synthesis routes (DCMS and HPPMS), are clearly reflected in their mechanical properties. Figure 4 illustrates the hardness (depicted on the left axis, represented by square symbols) and elastic modulus (depicted on the right axis, represented by circles) of the various $MoSi_2$ films.

The amorphous coating deposited at 200 °C exhibits low hardness (13.8 ± 0.7 GPa) in combination with a low elastic modulus (275 ± 20 GPa) [see Fig. 1(a)]. This finding aligns with the data presented by Chou and Nieh,[23] who determined a hardness of 10–12 GPa and a modulus of 225–232 GPa for amorphous sputtered $MoSi_2$ films. The elastic modulus exhibits a notable increase with the formation of the hexagonal $MoSi_2$ structure, reaching approximately 400 GPa for all crystalline $MoSi_2$-based films. In contrast, the hardness is found to exhibit a stronger dependence on the substrate temperature and the prevailing phases. The coatings deposited at 300 and 400 °C exhibit a peak hardness within the DCMS series, with values of 22.3 ± 1.6 and 21.4 ± 1.9 GPa, respectively. Subsequently, there is a notable decline in hardness to approximately 18 GPa at 600 °C. This finding is in good agreement with the phase evolution observed in Fig. 3 and the morphological

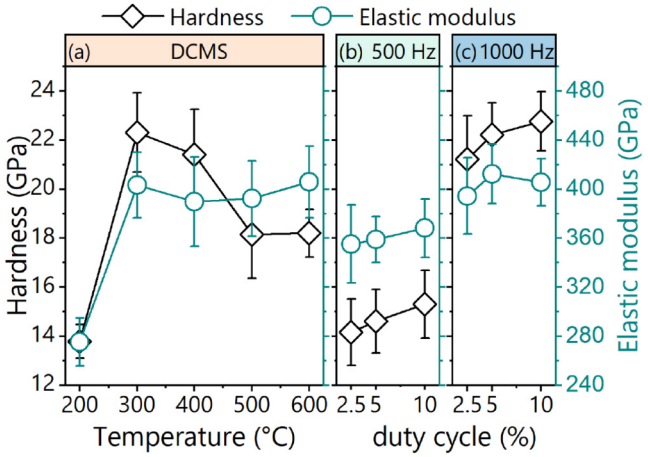

FIG. 4. Depiction of the hardness (on the left axis) and elastic modulus (on the right axis) of the (a) DCMS and (b) and (c) HPPMS coatings as a function of substrate temperature and duty cycle variation for different frequencies, 500 and 1000 Hz, respectively.

changes in Fig. 1. The formation of dual-phase structures (h-$MoSi_2$ and t-Mo_5Si_3) and larger grain/column sizes with underdense grain boundary regions, resulting from the enhanced surface diffusion, contribute to a decrease in hardness values. Nevertheless, it is challenging to discern the impact of orientation relations in the context of phase changes and overlapping peak positions.

For the HPPMS coatings, please refer to Figs. 4(b) and 4(c). The elastic modulus is approximately 400 GPa for the 1000 Hz series, which is comparable to the crystalline films produced by the DCMS series. Additionally, the 500 Hz series exhibits an elastic modulus of 360 GPa. The observed trend is in accordance with the phase evolution, as the 1000 Hz coatings and DCMS at 300 and 400 °C are predominantly randomly oriented h-$MoSi_2$ structured. The decline to 360 GPa for the predominantly t-Mo_5Si_3 structured 500 Hz series can be attributed to the phase transition. However, this phenomenon is not discernible for the DCMS coatings at temperatures ranging from 500 to 600 °C.

In terms of hardness, a more pronounced difference is evident between the two HPPMS series at 500 and 1000 Hz, as illustrated in Figs. 4(b) and 4(c). The highest hardness, 22.8 ± 1.2 GPa, is observed for an h-$MoSi_2$ structure coating grown at 1000 Hz and a duty cycle of 10%, respectively. In contrast, the same duty cycle at 500 Hz results in significantly lower hardness values, namely, 15.3 ± 1.4 GPa. The discrepancy of approximately 8 GPa between the two HPPMS series can be primarily attributed to their disparate morphologies. The films deposited at 1000 Hz exhibit a denser and finer morphology compared to those grown at 500 Hz (see also Fig. 2).

In addition to the observed morphological differences, the measured hardness and modulus values are also dependent on the crystal structure and texture. It was observed that films exhibiting dual-phase structures demonstrated lower hardness values than films displaying a predominant h-$MoSi_2$ phase and random orientation. The highest hardness values were observed for the DCMS thin film deposited at 300 °C and the 1000 Hz 10% duty cycle coating. Both exhibited an h-$MoSi_2$ dominated structure with a more or less random orientation but also contained the (100) orientation.

C. Oxidation characteristics

The objective of this investigation was to examine the long-term oxidation resistance of selected $MoSi_2$ films exposed to ambient air at temperatures of 600, 850, and 1200 °C for 100 h. To provide a variation in different morphologies and predominant crystal structures, two HPPMS coatings deposited at 500 and 1000 Hz, each with a 10% duty cycle, and the DCMS coating grown at 500 °C was selected for analysis. The 1000 Hz 10% duty cycle $MoSi_{1.92}$ is primarily h-$MoSi_2$ structured with a dense, small-grained morphology, as illustrated in Figs. 5(a)–5(c). In contrast, the DCMS coating grown at 500 °C [Figs. 5(d) and 5(e)] exhibits a dual-phase h-$MoSi_2$/t-Mo_5Si_3 structure with a partly open-porous morphology. Figures 5(g)–5(i) depict the dual-phase coating grown at 500 Hz and 10% duty cycle after oxidation at different temperatures. It is noteworthy that all of the coatings exhibited robust adhesion to the substrate (sapphire) throughout the oxidation process.

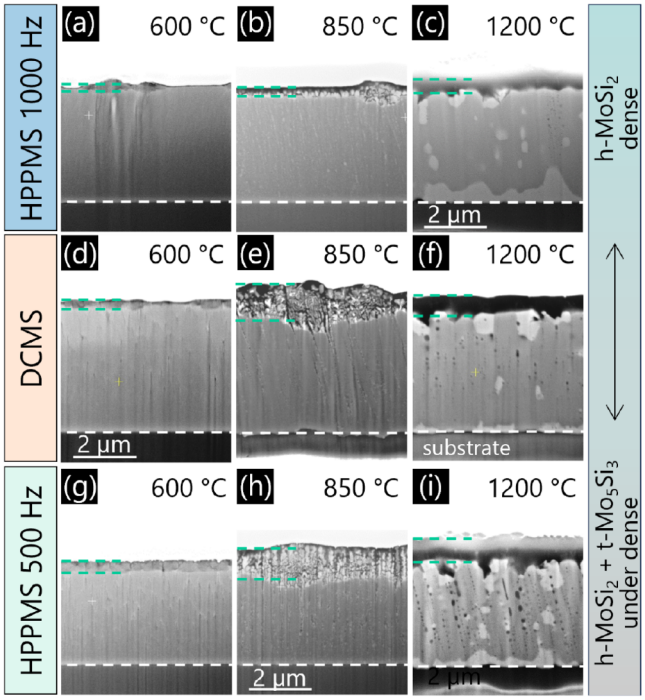

FIG. 5. FIB-prepared cross sections of isothermally oxidized $MoSi_2$ thin films grown on sapphire substrates for 100 h in ambient air at temperatures of 600, 850, and 1200 °C were analyzed. The first line depicts the HPPMS coating at 1000 Hz and a 10% duty cycle [(a) 600, (b) 850, and (c) 1200 °C], the middle row represents the DCMS coating deposited at 500 °C [(d) 600, (e) 850, and (f) 1200 °C], and the bottom row illustrates the HPPMS coating at 500 Hz and a 10% duty cycle, respectively [(g) 600, (h) 850, and (i) 1200 °C]. The interface between the substrate and the coating is indicated by a white dashed line. The oxide scale is delineated by two short, dashed lines.

Following the oxidation of the coatings at 600 °C for 100 h, an oxide layer was observed to form on the surface of all selected $MoSi_2$ coatings, as indicated by the turquoise dashed lines. It is notable that the 500 Hz HPPMS series sample, as illustrated in Fig. 5(g), exhibited the most substantial oxide layer, reaching approximately 400 nm in thickness. Furthermore, the film displayed a relatively underdense morphology and a low Si content of $MoSi_{1.86}$ in comparison to the DCMS sample (i.e., a Si/Mo ratio of 1.97) and the 1000 Hz sample (i.e., a Si/Mo ratio of 1.92). However, the $MoSi_{1.86}$ film is the only one to exhibit the formation of cracks within the oxide layer when subjected to oxidation at 600 °C. This behavior is consistent with the observed morphology and may indicate the presence of slight pesting phenomena. In this lower temperature range (approximately 600 °C), the interaction between MoO_x and SiO_x impedes the formation of a continuous, dense protective oxide layer. The disparities in thermal and volume expansion between these oxides contributed to the instability of the oxide scale, as evidenced by previous research.[8,31–33] Typically, the onset of pesting in $MoSi_2$ is triggered by local microstructural irregularities, such as cracks, pores, or grain boundaries, which subsequently

affect the entire sample. It is imperative to minimize these defects in $MoSi_2$ in order to prevent the pesting phenomenon.[34] During the pesting process, $MoSi_2$ may also decompose into so-called pest oxide products, which contain amorphous SiO_2 and MoO_x clusters.[33,34] These products were not observed at 600 °C. In contrast to the 500 Hz HPPMS sample, the DCMS $MoSi_{1.97}$ and the 1000 Hz $MoSi_{1.92}$ coating state exhibited enhanced resistance to crack formation and deterioration in oxidation behavior, which can be attributed to their superior structural, chemical, and particularly morphological design.

In contrast to the oxidation behavior observed at 600 °C, the coatings oxidized at 850 °C exhibit a slightly different behavior, with considerably thicker oxide scales. This is illustrated in Figs. 5(b), 5(e), and 5(h). In detail, the dual-phased states that are less dense [see Figs. 5(e) and 5(h)] demonstrate a notable increase in oxide scale thicknesses and an open porous scale formation. These observations are related to a slight pesting behavior, whereby the competing formation of MoO_x and SiO_x scales result in the formation of a rugged scale. The morphological appearance suggests that the SiO_x is glassy in nature and contains inclusions of molten MoO_x clusters (the melting point of MoO_3 is approximately 795 °C[35]). The HPPMS coating, which was grown at 1000 Hz and a 10% duty cycle, exhibited superior performance relative to the other coatings, as evidenced by a markedly reduced scale thickness. Nevertheless, it displayed a comparable scale formation pattern to the other coatings to a certain degree. In general, the oxide scales formed at 850 °C on the three different coatings do not appear completely dense at first glance. However, upon closer examination of the FIB cross sections, it becomes evident that the underlying coating is adequately protected, resulting in the $MoSi_2$-based coating surviving for up to 100 h.

At elevated temperatures (1200 °C), all $MoSi_2$-based coatings demonstrate exceptional oxidation resistance, which is attributed to the formation of a continuous, dense SiO_2 layer of approximately 500 nm. Any MoO_3 products that form at high temperatures evaporate rapidly (the boiling point of MoO_3 is approximately 1155 °C[35]), leaving a protective SiO_2 scale.[32,34] A comparison of the three oxidized samples at 1200 °C reveals notable contrasts with regard to the structural and morphological differences observed in the as-deposited state. Of particular note is the formation of pores, which was predominantly observed in the HPPMS 500 Hz 10% duty cycle sample [see Fig. 5(i)]. This phenomenon is attributed to the outward diffusion of silicon and the inward diffusion of oxygen along underdense column boundaries,[15] which is consistent with the observed slight underdense morphology. In contrast, the formation of pores was markedly diminished in the 1000 Hz sample subjected to 1200 °C, as illustrated in Fig. 5(c). This is also due to the notable improvement in the microstructure of the 1000 Hz series sample, as evidenced by a denser film in the as-deposited state [see Figs. 2(c) and 2(f)]. Furthermore, the lower Si content in the 500 Hz film results in a reduced capacity for Si to form a protective scale in comparison to the 1000 Hz film. A greater flux of Si outward diffusion is necessary for the formation of a protective SiO_2 scale. The DCMS coating [see Fig. 5(f)] exhibits an intermediate behavior, as the microstructure and phase evolution in the as-deposited state are well situated between the other two samples.

A further notable observation is the existence of discrete regions of darker and brighter appearing contrast within the residual $MoSi_2$ coating beneath the formed oxide scale. This effect is associated with the formation of Mo-rich Mo_5Si_3 (brighter areas based on mass contrast), which persists in the coating due to Si outward diffusion.[15] These observations indicate that the decomposition and phase formation of Mo_5Si_3 associated with Si deficiency can be observed not only during the deposition process (as evidenced by the 500 Hz and 500–600 °C DCMS states) but also during annealing treatments. This finding is substantiated by the observation that the as-deposited 1000 Hz 10% duty cycle coating is predominantly composed of h-$MoSi_2$ and that brighter Si-depleted areas form subsequent to the oxidation experiment [see Fig. 3(c)].

The presence of Mo-rich phase (Mo_5Si_3) in the long-term annealed coatings is further corroborated by XRD analysis. Figure 6 depicts the diffractograms of all long-term annealed samples at varying temperatures (600, 850, and 1200 °C) for 100 h.

Figure 6(a) provides a summary of the phase evolution of the long-term (100 h) oxidized 1000 Hz HPPMS sample. Following annealing at 600 °C, the $MoSi_2$ thin film continues to exhibit the metastable hexagonal $MoSi_2$ phase, with the presence of additional tetragonal Mo_5Si_3. Following annealing at 850 °C, a phase transition from hexagonal to the stable tetragonal $MoSi_2$ phase occurs. Even at 1200 °C, the stable tetragonal $MoSi_2$ phase remains the dominant phase, accompanied by the formation of the Mo_5Si_3 phase due to Si outward diffusion. Furthermore, additional minor peaks can be attributed to the cristobalite SiO_2 phase following annealing at 1200 °C. These peaks are distinctly present at diffraction angles (2Θ) of 21.9°, 31.5°, and 36.1° and are not superimposed upon any other peaks belonging to the tetragonal $MoSi_2$ or Mo_5Si_3 phase. The phase evolution resulting from the oxidation of the DCMS and 500 Hz HPPMS thin films is illustrated in Figs. 6(b) and 6(c), respectively. In general, a comparable trend is observed, albeit with slightly disparate initial conditions, as a result of the different phase constitution of the as-deposited state in comparison to the 1000 Hz HPPMS coating. Following oxidation at 600 °C, both coatings exhibited a mixture of h-$MoSi_2$ and t-Mo_5Si_3. It is notable that the HPPMS 500 Hz sample [Fig. 6(c)] retains a pronounced orientated structure, as evidenced by the peak at 41.5° that emerges following oxidation at 600 °C for 100 h in ambient air. Both the DCMS and the 500 Hz HPPMS coating then undergo the same phase transformation into tetragonal $MoSi_2$ after oxidation at 850 °C, with the additional Mo_5Si_3 still present. Following annealing at 1200 °C, the samples also exhibited the tetragonal $MoSi_2$ and Mo_5Si_3 peaks, as observed in the 1000 Hz HPPMS sample. Furthermore, the initial indications of a crystalline SiO_2 oxide layer can be identified through the presence of tetragonal cristobalite SiO_2 peaks.

To gain insights into extreme oxidation conditions, the HPPMS coating, which was grown at 500 Hz and a 10% duty cycle, was selected for investigation of its oxidation behavior and scale formation even at higher temperatures (1300, 1400, and 1500 °C). Despite the suboptimal initial condition, characterized by an underdense morphology and Si deficiency, the experiments should yield the exceptional oxidation behavior of $MoSi_2$-based coating. It should be noted that the measurement at 1500 °C was limited to

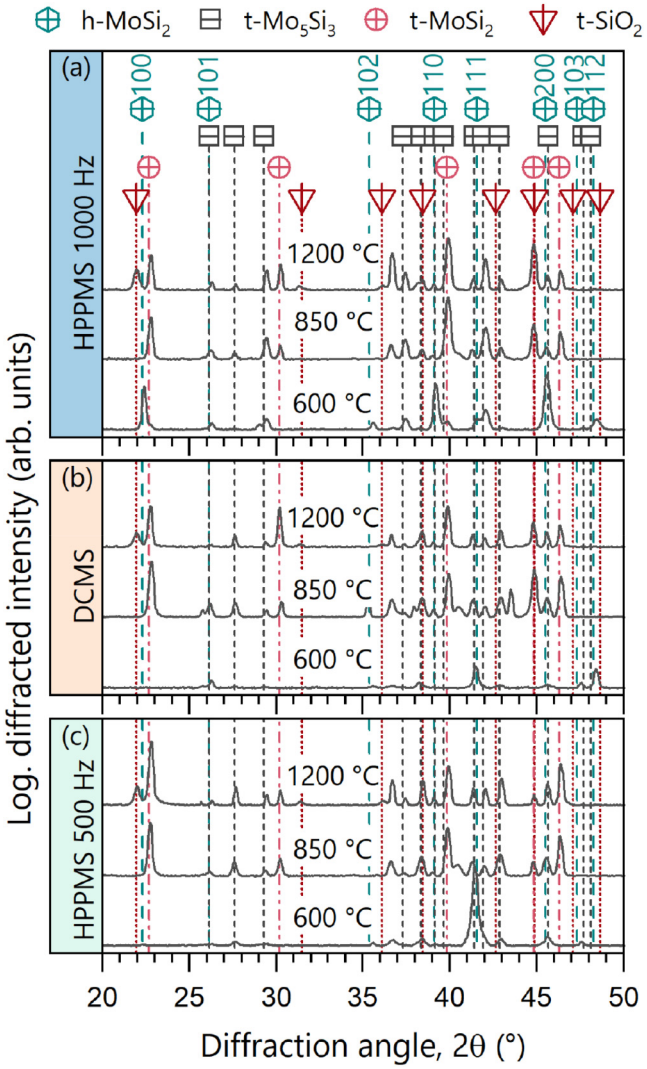

FIG. 6. X-ray diffractograms presented here depict the phase formation of long-term annealed $MoSi_2$-based coatings in ambient air for 100 h. The samples were annealed at 600, 850, and 1200 °C. Panel (a) depicts the diffractograms of the annealed 1000 Hz HPPMS films synthesized with a duty cycle of 10%, (b) of the annealed DCMS samples deposited at a substrate temperature of 500 °C, and (c) the data of the annealed 500 Hz films synthesized with a duty cycle of 10%. All measurements were conducted on coated single-crystalline Al_2O_3 substrates in Bragg–Brentano configuration with an offset of 3°. Hexagonal $MoSi_2$ is represented by hexagons (Ref. 29), tetragonal $MoSi_2$ by circles (Ref. 36), tetragonal Mo_5Si_3 by squares (Ref. 30), and tetragonal SiO_2 (cristobalite) by triangles. (Ref. 37).

30 min to protect the heating system, in comparison to 60 min for the other temperatures. Following the completion of the annealing tests, SEM cross sections were prepared and are presented in Fig. 7.

As illustrated in Fig. 7, the cross sections after oxidation demonstrate the exceptional oxidation resistance of the coating

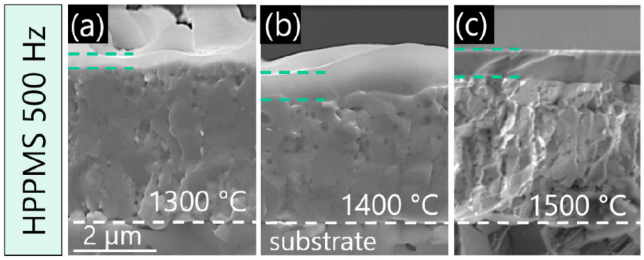

FIG. 7. SEM cross sections of an annealed $MoSi_2$-based thin film deposited on a polycrystalline Al_2O_3 substrate at 500 Hz and a duty cycle of 10%. Oxidation experiments were conducted in synthetic air at (a) 1300 °C (60 min), (b) 1400 °C (60 min), and (c) 1500 °C (30 min). The interface between the substrate and the coating is delineated by the white dashed line. The oxide scale formed is indicated by two short, dashed lines.

following exposure to these extreme conditions, despite a discernible substoichiometry of Si (Si/Mo ratio of 1.86). The thickness of the oxide layer exhibits a slight increase with elevated temperatures. The scale formation on the sample oxidized at 1300 and 1400 °C exhibits a glassy, wavy character, whereas the scale on the sample oxidized at 1500 °C displays a more uniform appearance. Additionally, the SEM images in Fig. 7 demonstrate minimal pore

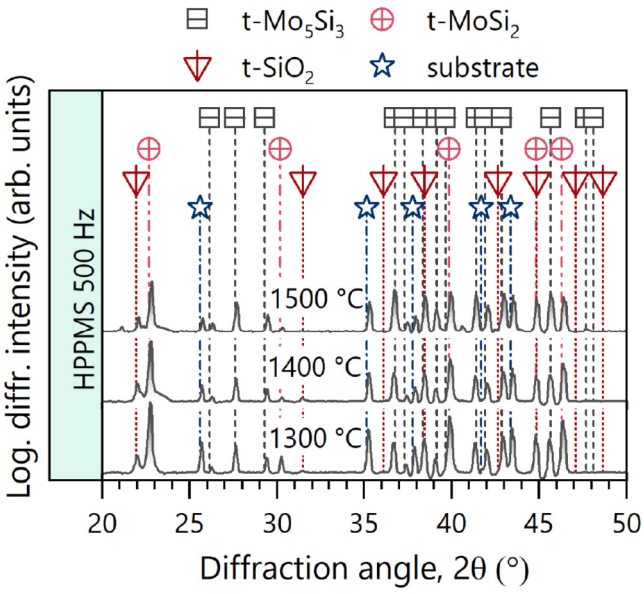

FIG. 8. X-ray diffractograms of oxidized $MoSi_2$-based coatings deposited at 500 Hz and a duty cycle of 10%. The oxidation experiments were conducted in synthetic air environment at 1300 °C (60 min), 1400 °C (60 min), and 1500 °C (30 min). All measurements were conducted on coated polycrystalline Al_2O_3 substrates [depicted by star symbols, as referenced in (Ref. 38)] utilizing a Bragg–Brentano configuration. The circles represent tetragonal $MoSi_2$ (Ref. 36), the squares represent tetragonal Mo_5Si_3 (Ref. 30), and the triangles represent tetragonal SiO_2 (cristobalite) (Ref. 37).

formation in comparison to the FIB-prepared cross section in Fig. 5(f), indicating an enhanced Si outward diffusion at elevated temperatures. Moreover, following isothermal testing at temperatures up to 1500 °C, all annealed coatings demonstrated robust adhesion to the polycrystalline Al_2O_3 substrate.

Following the high-temperature oxidation tests, the samples were also subjected to phase analysis. This was conducted to investigate the formation of oxide phases and to ascertain the phase stability of $MoSi_2$. As illustrated in Fig. 8, the XRD analysis clearly demonstrates the stability of the tetragonal $MoSi_2$ phase up to 1500 °C. Furthermore, the tetragonal Mo_5Si_3 phase was formed, as previously observed during the 100 h oxidation at 1200 °C. At all temperatures up to 1500 °C, the cristobalite SiO_2 phase could be clearly identified, particularly by the peaks at around 21.9°, 31.5°, and 36.1°, a peak shoulder at 42.6°, and possibly further overlapping peaks with the Mo_5Si_3 phase.

IV. CONCLUSIONS

The objective of this study was to conduct a comprehensive investigation on the phase formation, structure-mechanical properties, and high-temperature oxidation resistance of DCMS and HPPMS $MoSi_2$-based coatings. A particular emphasis was placed on the utilization of HPPMS in comparison to DCMS, which enabled the deposition of dense, h-$MoSi_2$ dominated thin films through the precise regulation of the ionization degree. Subsequently, the coatings were evaluated for their oxidation properties, which exhibited protective characteristics even at temperatures up to 1500 °C.

For DCMS, crystalline $MoSi_2$ films could be deposited at a substrate temperature of 300 °C and above, while x-ray amorphous films were only obtained below this temperature threshold. In their as-deposited state, films grown at temperatures between 300 and 400 °C predominantly crystallize in the hexagonal $MoSi_2$ structure. A higher substrate temperature (500–600 °C) is conducive to the formation of dual-phase coatings (h-$MoSi_2$ and t-Mo_5Si_3) and a Si substoichiometry. The 500 Hz HPPMS coatings exhibit a comparable phase formation and morphology to the DCMS coatings grown at 600 °C, predominantly featuring the additional t-Mo_5Si_3 structure and a pronounced columnar morphology. In contrast, the 1000 Hz HPPMS coatings are primarily composed of the h-$MoSi_2$ structure and exhibit a more randomly oriented texture.

The highest hardness was observed within the 1000 Hz HPPMS series for the random oriented h-$MoSi_{1.92}$ film, which exhibited a densely packed morphology, reaching 22.8 ± 1.2 GPa. The elastic modulus for all crystalline coatings was in the range of 360–400 GPa.

The oxidation behavior of the $MoSi_2$-based films was comprehensively investigated across a range of temperatures (650–1500 °C) over an extended period (up to 100 h). During oxidation at 600 °C, the formation of minor cracks in the oxide scales on top of the coatings was observed, indicating the presence of the pesting phenomenon. At 850 °C, the scales contain both amorphous SiO_x and MoO_x clusters, which are still indicative of a slight pesting-like behavior. The excellent oxidation resistance of $MoSi_2$ has been confirmed above 1200 °C, with an extremely thin scale of approximately 650 nm established for the HPPMS thin film deposited at a frequency of 1000 Hz with a 10% duty cycle. The formation of pores was markedly diminished through the strategic implementation of HPPMS. With regard to the outward diffusion of Si during oxidation, the formation of Mo_5Si_3-rich phase regions has been confirmed through structural analysis. Short-term tests (up to one hour) in the high temperature regime from 1300 to 1500 °C revealed effective protective oxidation mechanisms, namely, the formation of dense SiO_2 scales below 670 nm. This was observed even in films with a Si substoichiometry (Si/Mo ratio of 1.86).

The findings underscore the exceptional oxidation resistance up to 1500 °C and the valuable mechanical properties of nonreactively grown $MoSi_2$-based coatings, particularly for films deposited via HPPMS at 1000 Hz. In conclusion, the primary determinants of these remarkable properties are a predominant hexagonal $MoSi_2$ phase constitution and a highly dense microstructure.

ACKNOWLEDGMENTS

The financial support by the Austrian Federal Ministry for Digital and Economic Affairs, the National Foundation for Research, Technology and Development, and the Christian Doppler Research Association is gratefully acknowledged (Christian Doppler Laboratory "Surface Engineering of high-performance Components"). We also thank Plansee SE, Plansee Composite Materials GmbH, and Oerlikon Balzers, Oerlikon Surface Solutions AG for financial support. We also thank the X-ray center (XRC) of TU Wien for beam time and the electron microscopy center—USTEM TU Wien—for using the SEM and TEM facilities. Finally, we acknowledge TU Wien Bibliothek for financial support through its Open Access Funding Programme.

AUTHOR DECLARATIONS

Conflict of Interest

The authors have no conflicts to disclose.

Author Contributions

Sophie Richter: Conceptualization (lead); Data curation (lead); Formal analysis (lead); Investigation (lead); Methodology (lead); Project administration (equal); Visualization (lead); Writing – original draft (lead). **Ahmed Bahr:** Investigation (supporting); Methodology (supporting). **Philip Kutrowatz:** Investigation (supporting); Methodology (supporting). **Tomasz Wojcik:** Investigation (supporting); Methodology (supporting). **Szilárd Kolozsvári:** Funding acquisition (supporting); Writing – review & editing (supporting). **Peter Polcik:** Funding acquisition (supporting); Writing – review & editing (supporting). **Carmen Jerg:** Funding acquisition (supporting); Writing – review & editing (supporting). **Jürgen Ramm:** Funding acquisition (supporting); Writing – review & editing (equal). **Helmut Riedl:** Funding acquisition (lead); Project administration (equal); Supervision (lead); Writing – review & editing (equal).

DATA AVAILABILITY

The data that support the findings of this study are available from the corresponding author upon reasonable request.

REFERENCES

[1]L. Jiang, B. Zheng, C. Wu, P. Li, T. Xue, J. Wu, F. Han, and Y. Chen, Processes **10**, 1772 (2022).
[2]T. S. R. C. Murthy, B. Basu, A. Srivastava, R. Balasubramaniam, and A. K. Suri, J. Eur. Ceram. Soc. **26**, 1293 (2006).
[3]J. Lu, J.-B. Wang, S.-R. Yang, and Q.-J. Xue, Mocaxue Xuebao/Tribol. **23**(5), 361 (2003).
[4]F. Ferrieu, C. Viguier, A. Cros, A. Humbert, O. Thomas, R. Madar, and J. P. Senateur, Solid State Commun. **62**, 455 (1987).
[5]M. N. H. Liton, M. A. Helal, M. K. R. Khan, M. Kamruzzaman, and A. K. M. Farid Ul Islam, Indian J. Phys. **96**, 4155 (2022).
[6]A. A. Sharif, J. Mater. Sci. **45**, 865 (2010).
[7]Y. Q. Liu, G. Shao, and P. Tsakiropoulos, Intermetallics **9**, 125 (2001).
[8]D. A. Berztiss, R. R. Cerchiara, E. A. Gulbransen, F. S. Pettit, and G. H. Meier, Mater. Sci. Eng. A **155**, 165 (1992).
[9]S. Lohfeld and M. Schütze, Mater. Corros. **56**, 93 (2005).
[10]G. Sauthoff, *Intermetallics* (Wiley-VCH, Weinheim, Germany, 1995).
[11]J. J. Petrovic, MRS Bull. **18**, 35 (1993).
[12]S. Chevalier, F. Bernard, E. Gaffet, S. Paris, Z. A. Munir, and J. P. Larpin, "Effect of microstructure on the high temperature oxidation and pesting behaviour of $MoSi_2$," in *Materials Science Forum* (Trans Tech, Switzerland, 2004), pp. 439–446.
[13]H. J. Grabke and G. H. Meier, Oxid. Met. **44**, 147 (1995).
[14]F. Zhang, L. T. Zhang, A. D. Shan, and J. S. Wu, J. Alloys Compd. **422**, 308 (2006).
[15]A. Bahr *et al.*, J. Alloys Compd. **931**, 167532 (2023).
[16]E. K. Nyutu, M. A. Kmetz, and S. L. Suib, Surf. Coat. Technol. **200**, 3980 (2006).
[17]J. Yan, Y. Wang, L. Liu, Y. Wang, and F. Chen, J. Therm. Spray Technol. **24**, 1093 (2015).
[18]Y. Wang, D. Wang, J. Yan, and A. Sun, Appl. Surf. Sci. **284**, 881 (2013).
[19]X. Fei, Y. Niu, H. Ji, L. Huang, and X. Zheng, Ceram. Int. **37**, 813 (2011).
[20]J. Sun, T. Li, and G.-P. Zhang, Corros. Sci. **155**, 146 (2019).
[21]Y. Zhang, J. Zhao, J. Li, J. Lei, and X. Cheng, Ceram. Int. **45**, 5588 (2019).
[22]L. Liu, H. Q. Zhang, H. Lei, H. Q. Li, J. Gong, and C. Sun, Ceram. Int. **46**, 5993 (2020).
[23]T. C. Chou and T. G. Nieh, Thin Solid Films **214**, 48 (1992).
[24]P. V. Kiryukhantsev-Korneev and A. Potanin, Russ. J. Non-Ferr. Met. **59**, 698 (2018).
[25]W. Bretschneider and G. Beddies, Thin Solid Films **149**, 61 (1987).
[26]Plansee Composite Materials GmbH (2024).
[27]G. M. Pharr and W. C. Oliver, MRS Bull. **17**, 28 (1992).
[28]W. C. Oliver and G. M. Pharr, J. Mater. Res. **7**, 1564 (1992).
[29]International Center of Diffraction Data, Powder Diffraction File—hexagonal $MoSi_2$—04-018-0302 (2014).
[30]International Center of Diffraction Data, Powder Diffraction File—tetragonal Mo_5Si_3—04-005-9703 (2011).
[31]T. C. Chou and T. G. Nieh, JOM **45**, 15 (1993).
[32]C. Volders and P. Reinke, Surf. Sci. **681**, 134 (2019).
[33]T. C. Chou and T. G. Nieh, J. Mater. Res. **8**, 214 (1993).
[34]B. V. Cockeram, G. Wang, and R. A. Rapp, Oxid. Met. **45**, 77 (1996).
[35]American Elements (2024).
[36]International Center of Diffraction Data, Powder Diffraction File—tetragonal $MoSi_2$—00-006-0681 (1956).
[37]International Center of Diffraction Data, Powder Diffraction File—tetragonal SiO_2—00-011-0695 (1961).
[38]International Center of Diffraction Data, Powder Diffraction File—rhombohedral Al_2O_3—00-005-0712 (1955).